

# Synchronization Instability of Inverter-Based Generation During Asymmetrical Grid Faults

Xiuqiang He, *Student Member, IEEE*, Changjun He,  
Hua Geng, *Senior Member, IEEE*, and Feng Liu, *Senior Member, IEEE*

**Abstract**—Regardless of symmetrical or asymmetrical faults, transient stability of traditional power systems is concerned with the ability of generators to stay synchronized with the positive-sequence voltage of the network. In contrast, both positive- and negative-sequence synchronization should be of concern for inverter-based generation (IBG) during asymmetrical faults. This is because the latest grid codes stipulate that IBG should inject dual-sequence current when riding through asymmetrical faults. Currently, much less is known about the synchronization stability during asymmetrical faults. This significantly differs from the positive-sequence synchronization alone because the coupled dual-sequence synchronization is involved. This paper aims to fill this gap. Considering the sequence coupling under asymmetrical faults, the dual-sequence synchronization model of IBG is developed. Based on the model, the conditions that steady-state equilibrium points should follow are identified. The conditions throw light on the possible types of synchronization instability, including the positive sequence dominated instability and the negative-sequence dominated one. For different types of instability, the dominant factors are analyzed quantitatively, which are reflected by the limit on the current injection magnitude. Exceeding the limit will lead to the loss of synchronism in both the sequences. The model and the analysis are verified by simulations.

**Index Terms**—Asymmetrical fault, fault ride-through, grid code, grid-connected converter, loss of synchronism, stability conditions, transient stability, voltage-source converter.

## I. INTRODUCTION

RECENT years have witnessed a wide use of power electronic inverters as interface of renewable energy generation in the power system. Remaining in synchronism with the grid frequency is the foundation for the stable operation of inverter-based generation (IBG) [1]. Different from the intrinsic synchronizing mechanism dominated by synchronous generators, the synchronization of IBG is mainly accomplished by detecting and following the phase-angle of the terminal voltage. As the share of IBG is continuously rising in the power system, such grid-following mechanism has become one of the basic principles governing the synchronization behavior of the power system. For the IBG connected to a weak grid, in particular under grid faults, the terminal voltage is much sensitive. Thus, the synchronization may not be successfully achieved. The loss of synchronism (LOS) is manifested as the detected frequency significantly deviating from the grid fundamental frequency,

which can force the IBG to disconnect. In 2016 and 2017, 1,200 and 900 MW photovoltaic resource interruption events were caused by grid faults in California [2], [3]. It was reported that the disconnection partially resulted from the LOS [2], [3]. Such events had aroused wide concern over the LOS issue.

To avoid the loss of generation and provide ancillary support services, the IBG is required by mandatory grid codes to stay connected during grid faults and provide reactive current injection [4], [5]. In particular, asymmetrical fault-ride-through capability and dual-sequence current injection requirements have been stipulated by the German latest grid codes [5]. With the benefit of the dual-sequence current injection, the positive-sequence grid voltage can be supported and also the detrimental effects of the voltage imbalance can be reduced [6]. During the fault period, performing accurate reactive current injection necessities successful synchronization. Meanwhile, the synchronization behavior is also affected by the current injection as the IBG terminal voltage is subject to the voltage-current interaction on the grid impedance [7]–[9].

Under symmetrical grid faults, the positive-sequence synchronization is of concern. Most of existing synchronization stability studies were accomplished with the assumption that the grid fault is symmetrical [7]–[17]. The modeling in [9]–[11] revealed that the motion equation governing the synchronization behavior of IBG and synchronous generator shows a similar form. Consequently, the use of conventional transient stability analysis methods into the IBG synchronization stability research is inspired. Following this inspiration, the stability mechanism [9]–[14], the stability criterion [9]–[11] or stability boundary [11], [12], and the stability strategies [8]–[10], [15]–[17] have been comprehensively studied.

Asymmetrical faults are more frequent than symmetrical ones [6]. Under asymmetrical faults, the negative-sequence voltage appears in addition to the positive-sequence voltage. Both the positive- and negative-sequence synchronization is of importance, as required by the dual-sequence current injection [18], [19]. Regarding the ability of IBG to remain in synchronism with the grid frequency in both the positive and negative sequence after being subjected to a disturbance, it is referred to as *dual-sequence synchronization stability* in this paper. It is known that the sequence networks are interconnected under asymmetrical fault conditions. Therefore, the positive- and negative-sequence components are coupled (namely the sequence coupling) [20]. Owing to the sequence coupling, the stability mechanism of dual-sequence synchronization is much more complicated than that of positive-sequence synchronization alone. For the conventional power system, the transient stability assessment (TSA) under asymmetrical faults is similar

X. He, C. He, and H. Geng are with the Department of Automation, Beijing National Research Center for Information Science and Technology, Tsinghua University, Beijing, 100084, China (e-mail: he-xq16@mails.tsinghua.edu.cn; hcj20@mails.tsinghua.edu.cn; genghua@tsinghua.edu.cn).

F. Liu is with the State Key Laboratory of Power Systems, Department of Electrical Engineering, Tsinghua University, Beijing, 100084, China (e-mail: lfeng@tsinghua.edu.cn).

to that under symmetrical faults. This is due to the fact that only the positive-sequence synchronization is concerned. The impact of the negative- and zero-sequence networks is taken into account by inserting an additional impedance into the positive-sequence network [21]. Collectively, very little is currently known about the dual-sequence synchronization stability of IBG. It remains unclear how to characterize the dual-sequence synchronization behavior, what are the fundamental instability mechanism, and how to identify the stability conditions.

This paper aims to fill these gaps. By formulating the sequence voltage expression via the symmetrical components method, a dual-sequence synchronization model is developed. It is known that remaining in synchronism entails a feasible equilibrium point. Considering this fact, the stability analysis mainly focuses on the existence of stable equilibrium points. By looking into the conditions for the equilibrium points, the types of instability due to the absence of equilibrium points are defined. Then, the impact mechanism of current references, circuit parameters and fault types on different types of instability is investigated thoroughly, where the dominant instability factors are clarified and verified. The findings of this paper contribute to insightful understanding the LOS event occurring when IBG rides through asymmetrical grid faults.

The rest of this paper proceeds as follows. In Section II, an overview of a dual-sequence current-controlled IBG system is presented and the grid code requirements are reviewed. The system is modeled in Section III and the stability analysis is performed in Section IV. The conclusion is drawn in Section V.

## II. SYSTEM OVERVIEW AND GRID CODE REQUIREMENTS

The typical grid-connection topology and control diagram of the IBG system is illustrated in Fig. 1. In the latest grid codes, e.g., German grid code VDE-AR-N 4120 [5], it is required that the generation installed in the high-voltage network can ride through asymmetrical faults and provide dynamic reactive current support in the positive and negative sequence. To this end, the IBG system in Fig. 1 should perform dual-sequence reactive current injection during asymmetrical grid faults. By doing this, the positive-sequence voltage can be boosted while the negative-sequence voltage can be reduced [22]. During the fault period, the reactive current reference is specified according to the sequence voltage magnitude, as displayed in Fig. 2.

Under asymmetrical fault conditions, a synchronization unit should detect both the positive- and negative-sequence voltage vector position in order to simultaneously conduct the dual-sequence current control [18], [19]. Note that the negative-sequence control is dependent on the detection of the negative-sequence phase-angle, which cannot be replaced with the opposite of the positive-sequence phase-angle [18]. A commonly used synchronization unit is the dual second-order generalized integrator (DSOGI)-based phase-locked loop (DSOGI-PLL) or frequency-locked loop (DSOGI-FLL) [1], [23], which is depicted in Fig. 1(c). The DSOGI-PLL consists of the DSOGI quadrature signal generator (DSOGI-QSG) block, the positive- and negative-sequence calculation (PNSC) block and the PLL block. The DSOGI-QSG block is utilized to generate the orthogonal version (90°-lagging) of the input sig-

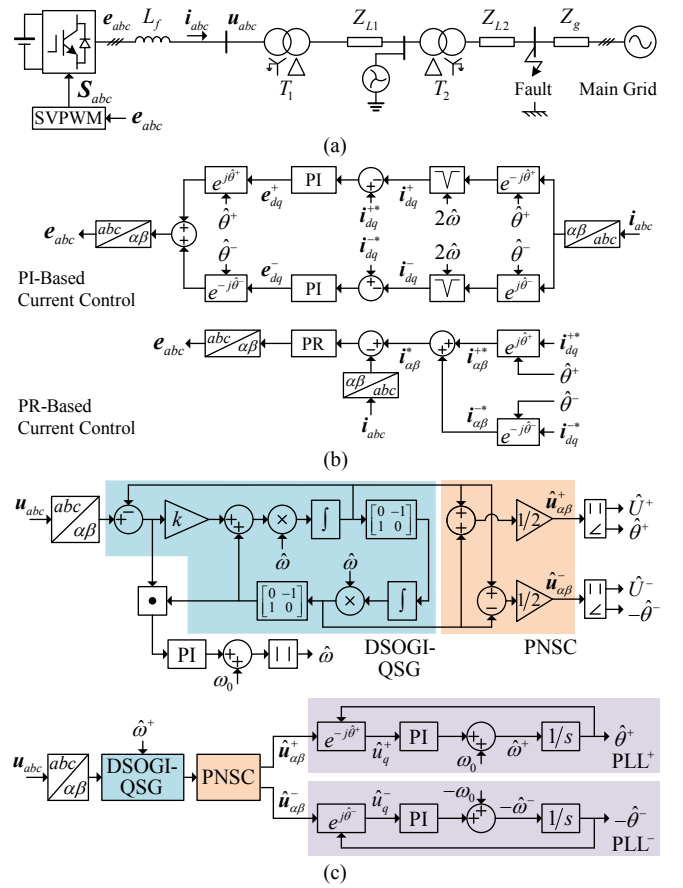


Fig. 1. Grid-connected IBG system under asymmetrical grid faults. (a) Circuit topology. (b) Proportional-integral (PI)-based or proportional-resonant (PR) regulator-based dual-sequence current control. (c) DSOGI-FLL/-PLL-based synchronization unit.

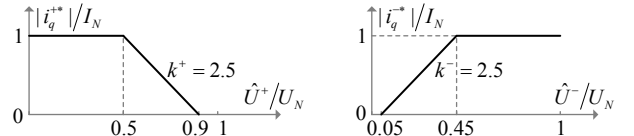


Fig. 2. Dual-sequence reactive current injection specifications based on the grid code [5].

nal. The sequence voltages are then obtained with the decomposition by the PNSC block. The positive-/negative-sequence phase-angle is finally observed by the PLL<sup>+</sup>/PLL<sup>-</sup> block, respectively. In the DSOGI-FLL, the phase-angle is calculated by algebraic manipulation instead.

It is noted again that the synchronization stability of the IBG system is concerned with the ability to remain in frequency synchronism with the grid *during the fault period*. This is distinguished from the transient stability of conventional power systems, where the post-fault synchronizing ability is of main concern. With this in mind, the modeling and stability analysis in this study is with respect to the *on-fault* period.

## III. SYSTEM MODELING

In Fig. 1, the grid-connection transformer  $T_2$  is generally of DYg type. Therefore, the high-voltage-side zero-sequence circuit is closed through the grounding connection of the neutral point. The low-voltage-side zero-sequence circuit is open

so that the zero-sequence component is absent [6]. Considering this fact, the IBG terminal phase voltages are assumed to be

$$\begin{bmatrix} u_a \\ u_b \\ u_c \end{bmatrix} = \begin{bmatrix} U^+ \cos(\omega t + \phi^+) + U^- \cos(\omega t + \phi^-) \\ U^+ \cos(\omega t - 2\pi/3 + \phi^+) + U^- \cos(\omega t + 2\pi/3 + \phi^-) \\ U^+ \cos(\omega t + 2\pi/3 + \phi^+) + U^- \cos(\omega t - 2\pi/3 + \phi^-) \end{bmatrix}. \quad (1)$$

The sequence voltage vectors (complex vectors) are denoted by  $\vec{U}^+ = U^+ e^{j(\omega t + \phi^+)}$ ,  $\vec{U}^- = U^- e^{-j(\omega t + \phi^-)}$ . The sequence voltage phasors are defined via the symmetrical components method as  $\dot{U}^+ = U^+ e^{j\phi^+}$ ,  $\dot{U}^- = U^- e^{j\phi^-}$ . The relationship between the vectors and the phasors are then expressed by [19],

$$\vec{U}^+ = \dot{U}^+ e^{j\omega t}, \quad \vec{U}^- = \dot{U}^- e^{j\omega t}. \quad (2)$$

The complex conjugate operation “\*” is applied to the negative-sequence voltage vector as it rotates clockwise with time, as shown in Fig. 3. The dual-sequence phase-angle positions estimated by the synchronization unit are represented by  $d^+$  and  $d^-$ . In the steady state,  $d^+$  and  $d^-$  coincide with the corresponding voltage vectors, thus giving the phasor diagram in Fig. 3 (c). While during dynamic conditions, both the estimated frequency and phase-angle exhibit some deviation. Additionally, the IBG terminal voltage changes with the output current during dynamic conditions. Therefore, the model characterizing the IBG synchronization behavior is composed of the terminal voltage representation and the synchronization unit.

#### A. Terminal Voltage Characterization

When investigating the large-signal synchronization stability, the current control dynamics and the electromagnetic transients can be neglected to simplify the modeling [9]–[13]. This simplification is justified with the fact that the synchronization dynamics are involved with the bandwidth of the synchronization unit, which is generally ten times smaller than the current controller bandwidth. Therefore, the synchronization dynamics can be approximately decoupled and analyzed separately in large-disturbance stability studies [9]–[13].

Without considering the current control dynamics, a quasi-steady-state current source can be used to represent the inverter. The orientation for the output current is provided by the synchronization unit. The angles are denoted by  $\hat{\theta}^+$  and  $-\hat{\theta}^-$ . The relative angles of the current vectors to the rotating reference frames are denoted by  $\theta_i^+$  and  $-\theta_i^-$ . Accordingly, the positive- and negative-sequence current outputs are defined by,

$$\begin{aligned} \vec{I}^+ &= I^+ e^{j(\hat{\theta}^+ + \theta_i^+)} \\ \vec{I}^- &= I^- e^{-j(\hat{\theta}^- + \theta_i^-)}. \end{aligned} \quad (3)$$

If the active current is zero, the positive-sequence reactive current output is overexcited and the negative-sequence one is underexcited, then  $\theta_i^+ = -\pi/2$ ,  $\theta_i^- = \pi/2$ , as seen in Fig. 4.

The phase-domain and sequence-domain circuits under any type of fault are shown in Fig. 5. Note that in addition to the winding configuration, the transformer model is also related to the composition and the core structure. A transformer composed of three single-phase transformers is considered here. The transformer phase shift is included in the circuit as it has an opposite effect on the positive- and negative-sequence voltages.

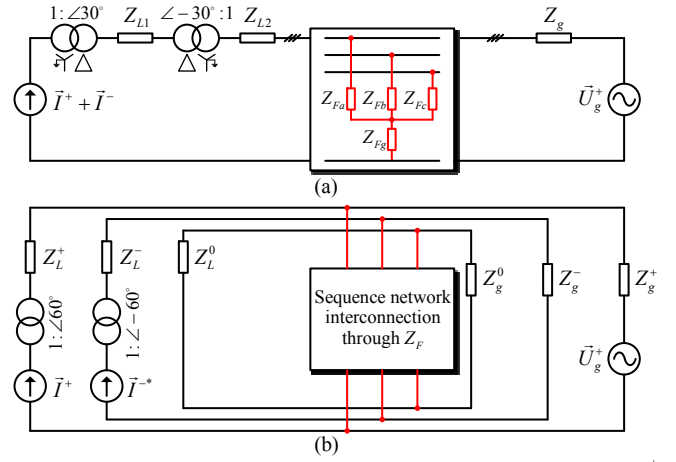


Fig. 5. (a) Phase-domain circuit. (b) Sequence-domain circuit, where  $Z_L^{\pm}$  consists of the sequence impedance of  $Z_{L1}$ ,  $Z_{L2}$  and of the two transformers whereas  $Z_L^0$  includes only the sequence impedance of  $Z_{L2}$  and of the transformer  $T_2$ . In view of the complete transposition of transmission lines, the positive- and negative-sequence line impedances are equal, denoted by  $Z_g^+ = Z_g^- = Z_g \angle \phi_g$ ,  $Z_L^+ = Z_L^- = Z_L \angle \phi_L$ . Subfigure (b) is detailed in Fig. 6.

TABLE I  
IMPEDANCE OF THE FAULT BRANCH

Fault type	$Z_{Fa}$	$Z_{Fb}$	$Z_{Fc}$	$Z_{Fg}$
SLG	0	$\infty$	$\infty$	$Z_F$
DLG	$\infty$	0	0	$Z_F$
LL	$\infty$	$Z_F/2$	$Z_F/2$	$\infty$

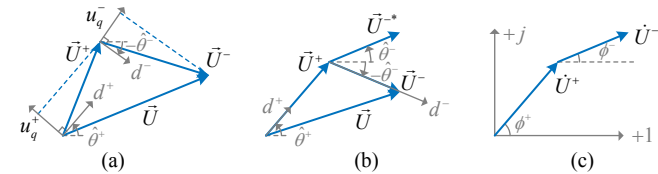


Fig. 3. (a) Voltage vectors and rotating reference frames during dynamic conditions, where  $\theta^+$  and  $-\theta^-$  are the phase-angles provided by the synchronization unit. (b)  $\theta^+ = \omega t + \phi^+$  and  $\theta^- = \omega t + \phi^-$  in the steady state. (c) Voltage phasors in the steady state.

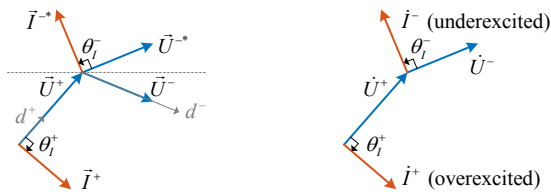


Fig. 4. Current vectors and phasors when injecting pure reactive current.

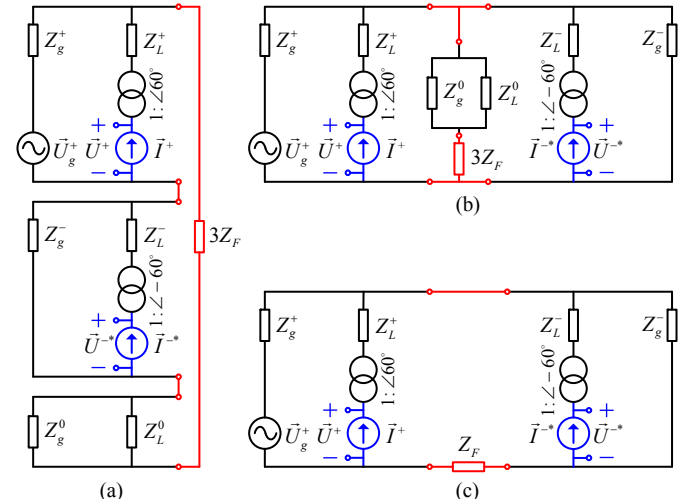


Fig. 6. Sequence-domain circuit under different types of faults. (a) SLG fault. (b) DLG fault. (c) LL fault.

Since the per-unit presentation is used, the transformation ratio is eliminated. It is suggested by (2) that the negative-sequence vector in Fig. 5(b) should be expressed in the form of complex conjugate. Also, it is seen that the occurrence of asymmetrical faults causes the coupling between the sequence components.

The fault impedance is summarized in Table 1 in the case of single line-to-ground (SLG) fault, double line-to-ground (DLG) fault, and line-to-line (LL) fault. Without loss of generality, phase A is considered as a special phase in the fault cases.  $Z_F$  is used to represent the fault impedance. Under different types of faults, the boundary conditions at the fault node can be formulated using the symmetrical components method [24]. Then, the sequence-domain circuit can be drawn, as seen in Fig. 6. Note that the presented circuit distinguishes itself from the conventional established one in the asymmetrical network analysis [24]. The major difference is that the dual-sequence current injection is incorporated in the circuit representation.

Based on the sequence-domain circuit, the inverter terminal sequence voltage can be represented. If it is assumed that the current reference remains constant during grid faults,  $I^+ e^{j\theta^+}$  and  $I^- e^{j\theta^-}$  will remain constant as well because the current control dynamics are neglected. Under this assumption, the voltage drop produced by  $\bar{I}^+$  on a branch with resistance  $R$  and inductance  $L$  is  $\Delta\bar{U}_Z^+ = R\bar{I}^+ + L d\bar{I}^+/dt = R\bar{I}^+ + j\hat{\omega}L\bar{I}^+ = Z\bar{I}^+$  [9], where  $Z = R + j\hat{\omega}L$ ,  $\hat{\omega}^+ = d\hat{\theta}^+/dt$ . Similarly, the voltage drop produced by  $\bar{I}^-$  is  $\Delta\bar{U}_Z^- = Z\bar{I}^-$ . In this way, the voltage equation of the circuit can be formed, as given by,

$$\bar{U}^+ e^{j\pi/3} = K_1 \bar{U}_g^+ + Z_2 \bar{I}^+ e^{j\pi/3} + Z_3 \bar{I}^- e^{-j\pi/3} \quad (4)$$

$$\bar{U}^- e^{-j\pi/3} = K_4 \bar{U}_g^+ + Z_5 \bar{I}^- e^{-j\pi/3} + Z_6 \bar{I}^+ e^{j\pi/3} \quad (5)$$

where  $K_i = |K_i| \angle \phi_i$ ,  $i = 1, 4$ ,  $Z_i = |Z_i| \angle \phi_i$ ,  $i = 2, 3, 5, 6$  are summarized in Table 2. In (4), (5), both the voltage components  $K_1 \bar{U}_g^+$  and  $K_4 \bar{U}_g^+$  are produced from the grid voltage  $\bar{U}_g^+$ . The latter is in fact resulted from the sequence network interconnection. Besides this, the sequence coupling is also characterized by the terms relevant to  $Z_3$  and  $Z_6$ . This coupling stems from the dual-sequence current injection and results in the interaction between the voltage and current components. Equations (4) and (5) further lead to (6) and (7),

$$\bar{U}^+ = |K_1| U_g^+ \angle(\phi_1 + \theta_g^+ - \pi/3) + |Z_2| I^+ \angle(\phi_2 + \hat{\theta}^+ + \theta_1^+) + |Z_3| I^- \angle(\phi_3 + \hat{\theta}^- + \theta_1^- - 2\pi/3) \quad (6)$$

$$\bar{U}^- = |K_4| U_g^+ \angle(\phi_4 + \theta_g^+ + \pi/3) + |Z_5| I^- \angle(\phi_5 + \hat{\theta}^- + \theta_1^-) + |Z_6| I^+ \angle(\phi_6 + \hat{\theta}^+ + \theta_1^+ + 2\pi/3) \quad (7)$$

The IBG terminal voltage is finally represented by,

$$\bar{U} = \bar{U}^+ + \text{conj}(\bar{U}^-) \quad (8)$$

## B. Synchronization Unit Modeling

The synchronization unit modeling has been well documented in the literature [1], [23]. The DSOGI-QSG block can be expressed in the form of complex vector by [23],

$$\begin{cases} d\hat{U}/dt = j\hat{\omega}\hat{V} + k\hat{\omega}(\bar{U} - \hat{U}) \\ d\hat{V}/dt = j\hat{\omega}\hat{U} \end{cases} \quad (9)$$

where  $\hat{U}$  and  $\hat{V}$  denote the filtered version and the 90° lagging version of the input signal  $\bar{U}$ , respectively. A frequency adaptive loop can be employed in the DSOGI-QSG block to adapt to the grid frequency variation, which is defined by [23],

$$\hat{\omega} = k_p \text{Im}[(\bar{U} - \hat{U})\hat{V}^*] + k_i \int_0^t \text{Im}[(\bar{U} - \hat{U})\hat{V}^*] d\tau + \omega_0. \quad (10)$$

The PNSC block is defined by,

$$\hat{U}^+ = 1/2(\hat{U} + \hat{V}), \quad \hat{U}^- = 1/2(\hat{U} - \hat{V}). \quad (11)$$

The PLL<sup>+</sup> and PLL<sup>-</sup> blocks are expressed by (12) and (13), respectively,

$$\begin{cases} d\hat{\theta}^+/dt = \hat{\omega}^+ \\ d\hat{\omega}^+/dt = k_p \hat{u}_q^+ + k_i \int \hat{u}_q^+ dt + \omega_0 \end{cases} \quad (12)$$

$$\begin{cases} d\hat{\theta}^-/dt = \hat{\omega}^- \\ d\hat{\omega}^-/dt = -k_p \hat{u}_q^- - k_i \int \hat{u}_q^- dt + \omega_0 \end{cases} \quad (13)$$

where  $\hat{u}_q^+$  and  $\hat{u}_q^-$  are the  $q$ -axis voltages, as seen in Fig. 3(a).

## C. Dual-Sequence Synchronization Model of the IBG System

By connecting the inverter voltage equation with the synchronization unit, the dual-sequence synchronization model is developed, as shown in Fig. 7. The developed model paves the way for quantitatively investigating the synchronization behavior of the dual-sequence current controlled IBG system. The

TABLE II  
THE EXPRESSIONS OF  $|K_i| \angle \phi_i$  AND  $|Z_i| \angle \phi_i$  UNDER DIFFERENT TYPES OF FAULTS

Symbol	SLG	DLG	LL	3LG
$K_1 =  K_1  \angle \phi_1$	$\frac{Z_g^- + Z_g^0 // Z_L^0 + 3Z_F}{Z_g^+ + Z_g^- + Z_g^0 // Z_L^0 + 3Z_F}$	$\frac{Z_g^0 // Z_L^0 + 3Z_F}{Z_g^+ + 2(Z_g^0 // Z_L^0) + 6Z_F}$	$\frac{Z_g^- + Z_F}{Z_g^+ + Z_g^- + Z_F}$	$\frac{Z_F}{Z_g^+ + Z_F}$
$Z_2 =  Z_2  \angle \phi_2$	$\frac{Z_g^+(Z_g^- + Z_g^0 // Z_L^0 + 3Z_F)}{Z_g^+ + Z_g^- + Z_g^0 // Z_L^0 + 3Z_F} + Z_L^+$	$\frac{Z_g^+(Z_g^0 // Z_L^0 + 3Z_F)}{Z_g^+ + 2(Z_g^0 // Z_L^0) + 6Z_F} + Z_L^+$	$\frac{Z_g^+(Z_g^- + Z_F)}{Z_g^+ + Z_g^- + Z_F} + Z_L^+$	$\frac{Z_g^+ Z_F}{Z_g^+ + Z_F} + Z_L^+$
$Z_3 =  Z_3  \angle \phi_3$	$-\frac{Z_g^+ Z_g^-}{Z_g^+ + Z_g^- + Z_g^0 // Z_L^0 + 3Z_F}$	$\frac{Z_g^+(Z_g^0 // Z_L^0 + 3Z_F)}{Z_g^+ + 2(Z_g^0 // Z_L^0) + 6Z_F}$	$\frac{Z_g^+ Z_g^-}{Z_g^+ + Z_g^- + Z_F}$	0
$K_4 =  K_4  \angle \phi_4$	$-\frac{Z_g^-}{Z_g^+ + Z_g^- + Z_g^0 // Z_L^0 + 3Z_F}$	$\frac{Z_g^0 // Z_L^0 + 3Z_F}{Z_g^+ + 2(Z_g^0 // Z_L^0) + 6Z_F}$	$\frac{Z_g^-}{Z_g^+ + Z_g^- + Z_F}$	0
$Z_5 =  Z_5  \angle \phi_5$	$\frac{Z_g^-(Z_g^+ + Z_g^0 // Z_L^0 + 3Z_F)}{Z_g^+ + Z_g^- + Z_g^0 // Z_L^0 + 3Z_F} + Z_L^-$	$\frac{Z_g^-(Z_g^0 // Z_L^0 + 3Z_F)}{Z_g^- + 2(Z_g^0 // Z_L^0) + 6Z_F} + Z_L^-$	$\frac{Z_g^-(Z_g^+ + Z_F)}{Z_g^+ + Z_g^- + Z_F} + Z_L^-$	0
$Z_6 =  Z_6  \angle \phi_6$	$-\frac{Z_g^+ Z_g^-}{Z_g^+ + Z_g^- + Z_g^0 // Z_L^0 + 3Z_F}$	$\frac{Z_g^+(Z_g^0 // Z_L^0 + 3Z_F)}{Z_g^- + 2(Z_g^0 // Z_L^0) + 6Z_F}$	$\frac{Z_g^+ Z_g^-}{Z_g^+ + Z_g^- + Z_F}$	0

model is general to any short-circuit fault type. In this sense, the previously established model with respect to symmetrical grid faults [9] is a special case of this general model.

The accuracy of the model is verified by comparison with a detailed simulation model. The results are shown in Fig. 8. It is seen that the proposed model is able to approximate the detailed model quite well. In the steady state during the fault period, in particular, the results of the two models are highly coincident, which verifies the correctness the voltage equation. Note that there is some deviation at the moment of the fault occurrence and clearance. This is because the current control dynamics and nonlinear components such as current saturation are neglected in the proposed model.

It is worth reminding that a dual-sequence synchronization model has been reported in [25] lately. However, it was shown in [25] that the model exhibits some steady-state error. This was in fact due to the improper use of the sequence network split to derive the Thevenin equivalents. As a consequence, the sequence network interconnection was broken and the circuit operating point was also altered in the derivation. The steady-state error is addressed in the model developed here by avoiding using the sequence network split.

#### IV. SYNCHRONIZATION STABILITY ANALYSIS

The IBG is supposed to remain in synchronism with the grid during the fault period. To achieve this, one should make sure at first that a feasible steady-state operating point is available. On this basis, the domain of attraction can be investigated further [11], [12]. In this study, the stability analysis mainly focuses on the characteristics of steady-state equilibrium points.

##### A. Conditions for Equilibrium Points

Using  $e^{-j\hat{\theta}^+}$ ,  $e^{-j\hat{\theta}^-}$  to transform (6), (7) into the rotating reference frames leads to (14), (15), respectively,

$$u_d^+ + ju_q^+ = |K_1|U_g^+ \angle(\phi_1 - \delta^+) + |Z_2|I^+ \angle(\phi_2 + \theta_1^+) + |Z_3|I^- \angle(\phi_3 + \theta_1^- - \delta^+ + \delta^-) \quad (14)$$

$$u_d^- - ju_q^- = |K_4|U_g^+ \angle(\phi_4 - \delta^-) + |Z_5|I^- \angle(\phi_5 + \theta_1^-) + |Z_6|I^+ \angle(\phi_6 + \theta_1^+ + \delta^+ - \delta^-) \quad (15)$$

where  $\delta^+ = \hat{\theta}^+ - \theta_g^+ + \pi/3$ ,  $\delta^- = \hat{\theta}^- - \theta_g^- - \pi/3$ . In the steady state (if it exists),  $u_q^\pm = 0$  and  $u_d^\pm > 0$  are the basic requirements for the voltage vector orientation, i.e.,

$$\begin{cases} |K_1|U_g^+ \sin(\phi_1 - \delta^+) + |Z_2|I^+ \sin(\phi_2 + \theta_1^+) + |Z_3|I^- \sin(\phi_3 + \theta_1^- - \delta^+ + \delta^-) = 0 \\ |K_4|U_g^+ \sin(\phi_4 - \delta^-) + |Z_5|I^- \sin(\phi_5 + \theta_1^-) + |Z_6|I^+ \sin(\phi_6 + \theta_1^+ + \delta^+ - \delta^-) = 0. \end{cases} \quad (16)$$

$$\begin{cases} |K_1|U_g^+ \cos(\phi_1 - \delta^+) + |Z_2|I^+ \cos(\phi_2 + \theta_1^+) + |Z_3|I^- \cos(\phi_3 + \theta_1^- - \delta^+ + \delta^-) > 0 \\ |K_4|U_g^+ \cos(\phi_4 - \delta^-) + |Z_5|I^- \cos(\phi_5 + \theta_1^-) + |Z_6|I^+ \cos(\phi_6 + \theta_1^+ + \delta^+ - \delta^-) > 0 \end{cases} \quad (17)$$

The physical meaning of (16) and (17) is interpreted as follows. The IBG is represented with a current source. The terminal voltage and the output current are subject to Kirchhoff's laws while the output current control is bound by the voltage orientation. If the solution for  $\delta^+$  and  $\delta^-$  is nonexistent, the

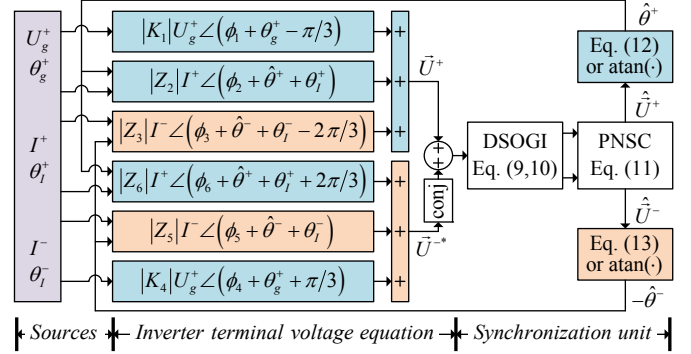


Fig. 7. Proposed model for investigating the dual-sequence synchronization stability of the IBG system.

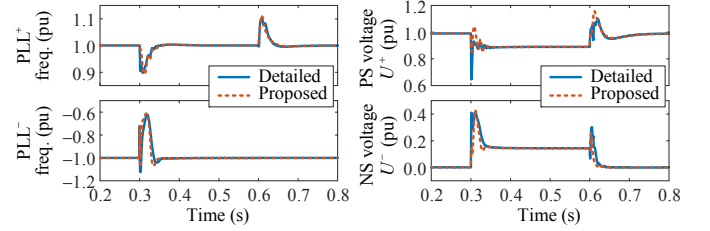


Fig. 8. Verification results of the proposed model under the SLG fault. Note that the model has also been verified under the DLG and LL fault.

dual-sequence synchronization along with the current control cannot be fulfilled. This will consequently result in the LOS. Therefore, the nonexistence of steady-state equilibrium points is one of the underlying causes of synchronization instability.

Generally, as long as there are solutions to meet both (16) and (17), the solutions can be classified into stable equilibrium points and unstable equilibrium points according to the symmetry of trigonometric function [16]. In other words, as long as there are equilibrium points, there should be a stable equilibrium point. The point can be identified with the negative feedback condition of the synchronization unit,  $du_q^+/d\delta^+ < 0$ ,  $-du_q^-/d\delta^- < 0$ , i.e.,

$$\begin{cases} -|K_1|U_g^+ \cos(\phi_1 - \delta^+) - |Z_3|I^- \cos(\phi_3 + \theta_1^- - \delta^+ + \delta^-) < 0 \\ -|K_4|U_g^+ \cos(\phi_4 - \delta^-) - |Z_6|I^+ \cos(\phi_6 + \theta_1^+ + \delta^+ - \delta^-) < 0. \end{cases} \quad (18)$$

The conditions that stable equilibrium points should follow are proposed by (16) to (18). By numerically solving (16) under the constraints of (17) and (18), the on-fault steady-state point can be calculated. To facilitate an intuitive understanding of the steady-state point, the phasor diagram is drawn, as depicted in Fig. 9, where the circuit parameters is provided in Table 3. As expected, the positive-sequence terminal voltage is boosted with the overexcited current injection; the negative-sequence one is reduced with the underexcited current injection. Also, it is important to note that the sequence coupling is counterproductive to the voltage boost and reduction. This is manifested as  $|Z_3|I^- \angle(\phi_3 + \theta_1^- + \delta^-)$  reacting against  $|K_1|U_g^+ \angle\phi_1$  whereas  $|Z_6|I^+ \angle(\phi_6 + \theta_1^+ + \delta^+)$  enhancing support for  $|K_4|U_g^+ \angle\phi_4$ .

As disclosed by the previous research [26], the absence of the equilibrium point implies that the closed polygon in Fig. 9 cannot be formed by the phasor synthesis. This can lead to an inappropriate interaction appearing between the controllers and the circuit impedance [26]. The interaction cannot settle down

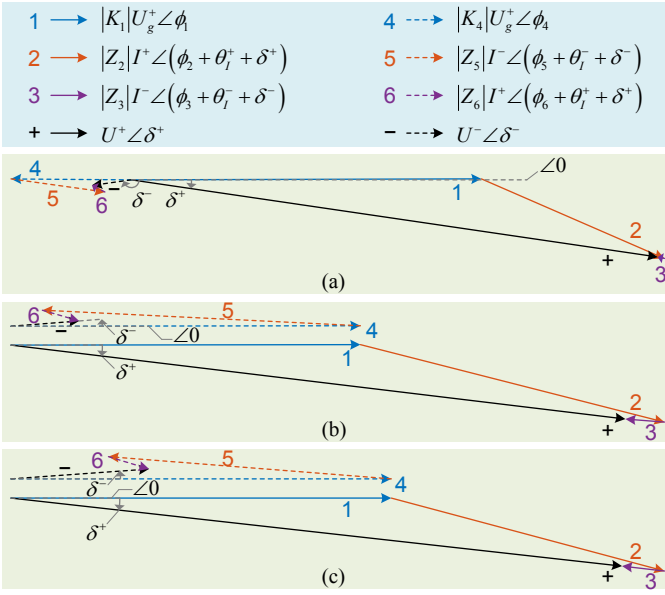


Fig. 9. Phasor diagram in the on-fault steady state. (a) SLG fault. (b) DLG fault. (c) LL fault. In the SLG fault,  $I^+ \angle \theta_t^+ = 0.6 \angle -90^\circ$ ,  $I^- \angle \theta_t^- = 0.3 \angle 90^\circ$ . In the DLG and LL fault,  $I^+ \angle \theta_t^+ = 0.6 \angle -90^\circ$ ,  $I^- \angle \theta_t^- = 0.6 \angle 90^\circ$ .

TABLE III  
SYSTEM PARAMETERS

Symbol	Description	Value
$U_N$	Voltage level	110 kV / 35 kV / 690 V
$U_g$	Grid voltage	120 kV
$S_N$	Nominal capacity	9 MVA
$f_n$	Nominal frequency	50 Hz
$R_c + jX_c$	Choke impedance	0.15/50 + j0.15 p.u.
$Z_{T1}^+ (= Z_{T1}^- = Z_{T1}^0)$	$T_1$ impedance	0.06/30 + j0.06 p.u.
$Z_{T2}^+ (= Z_{T2}^- = Z_{T2}^0)$	$T_2$ impedance	0.16/30 + j0.16 p.u.
$Z_{L1}^+ (= Z_{L1}^- = Z_{L1}^0/3)$	$Z_{L1}$ impedance	0.02 + j0.05 p.u.
$Z_{L2}^+ (= Z_{L2}^- = Z_{L2}^0/3)$	$Z_{L2}$ impedance	0.06 + j0.3 p.u.
$Z_g^+ (= Z_g^- = Z_g^0/3)$	$Z_g$ impedance	0.04 + j0.2 p.u.
$Z_F$	Fault impedance	0.01 $\Omega$
$k$	Gain of SOGI unit	1.414
$K_{p\_PLL}, K_{i\_PLL}$	PLL PI parameters	100, 2000
$K_{p\_Curr}, K_{r\_Curr}$	PR parameters	12, 1000

due to the absence of equilibrium points, thus followed by a transient instability phenomenon. It should be noted that as long as one of the conditions in (16) to (18) cannot be followed, both the dual-sequence current control will lose synchronism. This is due to the sequence coupling effect. From the phasor diagram in Fig. 9, it is indicated that the instability is related to the fault type, current references, and the circuit parameters. A comprehensive investigation on the possible instability types and dominant factors is lunched below.

### B. Instability Types and Dominant Factors

Owing to the complexity of trigonometric function, figuring out the explicit conditions for one specific parameter is a non-trivial task. For this reason, the dominant instability factors will be ascertained by a decoupling analysis at first. Then the impact of the sequence coupling on the stability will be investigated.

In Table 2,  $Z_2$  and  $Z_5$  contain the grid-connection impedance  $|Z_L|$ . The size of  $|Z_2|$  and  $|Z_5|$  is therefore much larger than that of  $|Z_3|$  and  $|Z_6|$ , especially in a weak connection scenario, as indicated by the phasor diagram in Fig. 9. Ne-

glecting the sequence coupling terms involving  $Z_3$  and  $Z_6$  in (16), the conditions for the existence of equilibrium points can be formulated explicitly, as given by (19),

$$|Z_2| I^+ \sin|\phi_2 + \theta_t^+| \leq |K_1| U_g^+ \Rightarrow I_{\text{lim}}^+ = \frac{|K_1| U_g^+}{|Z_2| \sin|\phi_2 + \theta_t^+|} \quad (19a)$$

$$|Z_5| I^- \sin|\phi_5 + \theta_t^-| \leq |K_4| U_g^+ \Rightarrow I_{\text{lim}}^- = \frac{|K_4| U_g^+}{|Z_5| \sin|\phi_5 + \theta_t^-|} \quad (19b)$$

where the boundary conditions are expressed by the limit on the current injection magnitude. Analogously, neglecting the sequence coupling terms in (17) and then combining with (16) can formulate the other part of the boundary conditions:

$$|Z_2| I_{\text{lim}}^+ = |K_1| U_g^+ \Rightarrow I_{\text{lim}}^+ = |K_1| U_g^+ / |Z_2| \quad (20a)$$

$$|Z_5| I_{\text{lim}}^- = |K_4| U_g^+ \Rightarrow I_{\text{lim}}^- = |K_4| U_g^+ / |Z_5| \quad (20b)$$

The boundary conditions are exemplified in Figs. 10 and 11, where the shadow area represents the allowable region for the current injection. The solid-line boundary of Regions 1 and 3 is defined by (19a) and (19b), respectively. The dashed-line boundary of Regions 2 and 4 is defined by (20a) and (20b), respectively. Observing these boundaries, the instability types and dominant factors can be summarized as follows.

1) *Positive Sequence Dominated Type-1 Instability*: i.e., the instability due to the positive-sequence current injection going beyond the boundary of Region 1. As seen in Fig. 10(b), assuming the voltage vector  $\bar{U}^+$  rotates to the zero-degree angle at a certain moment, the impedance voltage drop  $Z_2 I_{\text{lim}}^+$  can be drawn under the current injection  $\bar{I}_{\text{lim}}^+$ . Centered on the tip point of  $Z_2 \bar{I}_{\text{lim}}^+$ , a circle with radius equal to  $|K_1| U_g^+$  is drawn. At the critical operating point, the circle is tangent to the zero-degree horizontal line. If the current magnitude increases to exceed the limit, the horizontal line will fail to intersect with the circle and consequently there will be no steady-state operating points. For this type of instability, the dominant factors are reflected by the current injection limit in (19a). In particular, the smaller the ratio  $|K_1| U_g^+ / |Z_2|$  is, the smaller the allowable operating region as well. This suggests that both a severe grid fault and a weak grid connection are detrimental to the synchronization stability.

2) *Positive Sequence Dominated Type-2 Instability*: i.e., the instability due to the positive-sequence current injection going beyond the boundary of Region 2. As depicted in Fig. 10(c), the voltage component  $K_1 \bar{U}_g^+ e^{-j\pi/3}$  is counterbalanced by the impedance voltage drop, i.e., the terminal voltage is reduced to zero. The current injection exceeding the limit is disallowed as it leads to a reverse (180-degree) terminal voltage vector. This will mislead and destabilize the voltage-oriented current control. The dominant factors of this instability type are reflected by the current injection limit in (20a). In contrast to the type-1 instability,  $\phi_2 + \theta_t^+$  has no effect on the limit here.

3) *Negative Sequence Dominated Type-1 Instability*: i.e., the instability due to the negative-sequence current injection going beyond the boundary of Region 3. The critical operating point is demonstrated in Fig. 11(b). The dominant instability factors are reflected by the current injection limit in (19b), where the ratio  $|K_4| U_g^+ / (|Z_5| \sin|\phi_5 + \theta_t^-|)$  plays an important role in affecting the existence of equilibrium points. Due to

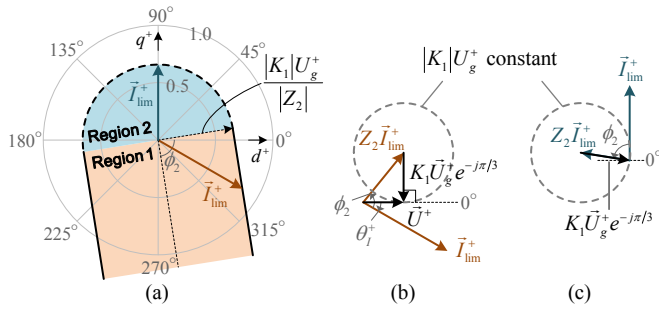


Fig. 10. (a) Allowable region for the positive-sequence current injection during a DLG-type fault. (b) For  $\bar{I}_{lim}^+$  in Region 1,  $|K_1|U_g^+$  matches just enough  $Z_2\bar{I}_{lim}^+$  in the vertical direction. (c) For  $\bar{I}_{lim}^+$  in Region 2, the terminal voltage is reduced to zero just right.

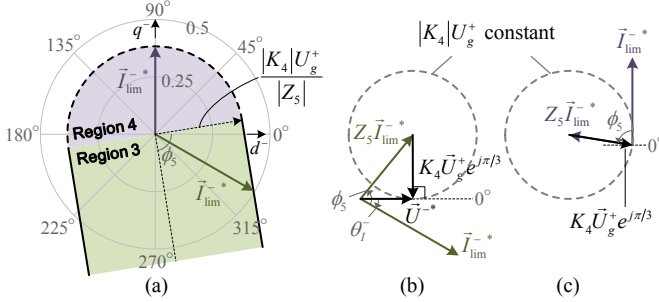


Fig. 11. (a) Allowable region for the negative-sequence current injection during a SLG-type fault. In (b) and (c), the critical operating points are explained similarly to those in Fig. 10.

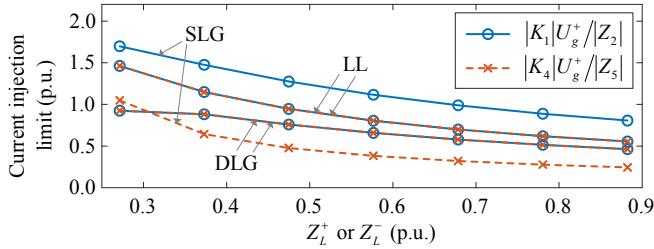


Fig. 12. Comparisons of the current injection limit under different fault types and different line impedances.

$|K_4| \leq |K_1|$  whereas  $|K_2| = |K_5|$ , this type of instability is more likely than the positive sequence dominated type-1 instability. This is the case under the SLG-type fault, as demonstrated by Fig. 12.

4) *Negative Sequence Dominated Type-2 Instability*: i.e., the instability due to the negative sequence current injection going beyond the boundary of Region 4. Similarly, the boundary is shaped by the critical operating points where the negative-sequence voltage is reduced to zero. Moreover, the ratio  $|K_4|U_g^+/|Z_5|$  proves to be the dominant instability factors.

Four types of instability and the dominant factors have been clarified, which gives insights into the impact mechanism of the current injection and the circuit impedances on the steady-state allowable operating region. In some of current grid codes, it is important to note that the current injection is specified in the positive sequence only. This is actually a special case of the above analysis as only the positive sequence dominated type-1 and type-2 instability is involved. Note also that the operating range exemplified in Figs. 10 and 11 is with respect to the DLG and SLG fault types, respectively. The comparisons between

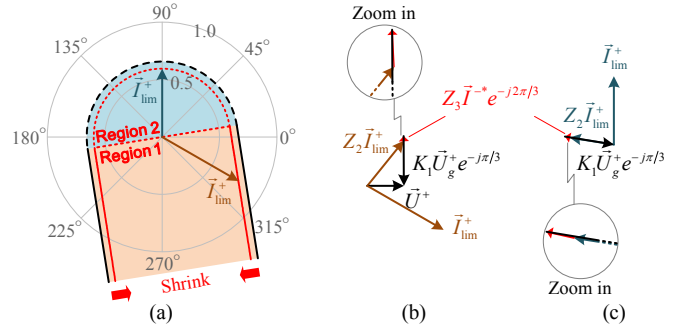


Fig. 13. (a) The allowable region for the positive-sequence current injection shrinks when considering the impact of a negative-sequence current injection,  $I^+ \angle \theta_f^+ = 0.5 \angle 90^\circ$ . (b) and (c) show the vector diagrams depicting the equilibrium points on the boundary.

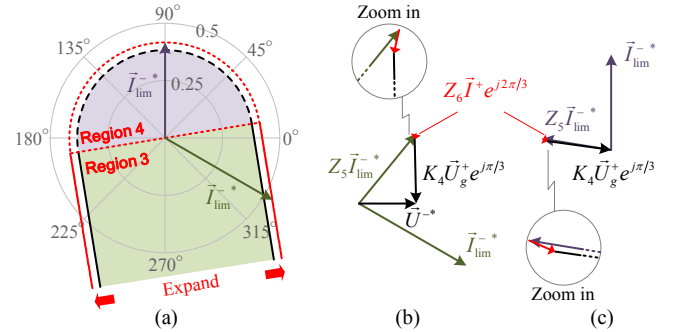


Fig. 14. (a) The allowable region for the negative-sequence current injection expands when considering the impact of a positive-sequence current injection,  $I^+ \angle \theta_f^+ = 0.5 \angle -90^\circ$ . (b) and (c) show the vector diagrams depicting the equilibrium points on the boundary.

different fault types are displayed in Fig. 12. As reflected by the ratio, the positive-sequence dominated instability is more likely to occur under the DLG-type fault compared to the other two types of fault. Furthermore, the SLG-type fault most easily suffers from the negative-sequence dominated instability.

### C. Impact of the Sequence Coupling on the Stability

When considering the sequence coupling effect, the current injection limit can be identified using a traversal algorithm with the help of numerical computation. In Fig. 13, the allowable range for the positive-sequence current injection shrinks when injecting a negative-sequence underexcited current at the same time. In Fig. 14, on the contrary, the allowable range for the negative-sequence current injection expands when injecting a positive-sequence overexcited current additionally. The vector diagrams depicting the critical operating points are shown in the subfigures (b) and (c). As displayed in Fig. 13, the negative-sequence underexcited current injection produces a counteracting effect on  $K_1\bar{U}_g^+e^{-j\pi/3}$ , therefore reducing the positive-sequence current injection limit. In Fig. 14, the positive-sequence overexcited current injection provides a supporting effect on  $K_4\bar{U}_g^+e^{j\pi/3}$ , therefore improving the negative-sequence injection limit. Both of these two aspects are attributable to the sequence coupling and they are also identical with the observation from the phasor diagram in Fig. 9.

The boundary in Figs. 13 and 14 have also been verified by simulations on a detailed model, where the parameters in Table 3 are adopted. Considering  $\bar{I}_{lim}^+ = 0.768 \angle -30^\circ$  in Fig. 13 as an

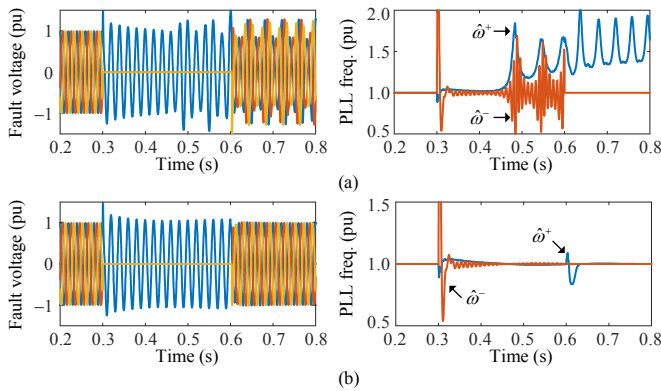


Fig. 15 (a) Dual-sequence synchronization instability is observed when injecting  $\hat{I}^+ = 0.77\angle -30^\circ$  beyond the boundary of Region 1. It is seen that the instability is dominated by the loss of the positive-sequence synchronism. (b) The instability is avoided, where  $\hat{I}^+ = 0.75\angle -30^\circ$ .

example, it is shown in Fig. 15(a) that if the current injection exceeds the limit, the IBG system will undergo the positive sequence dominated type-1 instability. In Fig. 15(b), it is verified that the instability is avoided, where the magnitude of the positive-sequence current injection is slightly reduced.

## V. CONCLUSION

This paper aims to study the dual-sequence synchronization stability of IBG under asymmetrical grid fault conditions. The main contributions are summarized as follows: 1) A dual-sequence synchronization model was proposed for the IBG under asymmetrical fault conditions. 2) Based on the model, the essential conditions for the IBG synchronization stability were identified by looking into the existence of equilibrium points. 3) According to the stability conditions, the instability types were defined and analyzed, and the dominated instability factors were quantified with the current injection limit.

The findings show that the LOS of a dual-sequence current-controlled IBG signifies that both the positive and negative sequence suffer from instability. The instability, however, is generally dominated by one sequence. The positive sequence dominated instability is more likely to occur under the DLG fault whereas the negative sequence dominated one is more likely to occur under the SLG fault. In addition, the positive-sequence current injection limit is affected by the current injection in the negative sequence and vice versa. The sequence coupling effects caused by the overexcited and underexcited current injection are also opposite. These findings suggest that a tradeoff should be considered in assigning the positive- and negative-sequence reactive current. This will be an important consideration in the amendments of future grid codes. Based on the findings, the future attention will be directed to the dynamic synchronization behavior.

## REFERENCES

- [1] S. Golestan, J. M. Guerrero, and J. C. Vasquez, "Three-phase PLLs: a review of recent advances," *IEEE Trans. Power Electron.*, vol. 32, no. 3, pp. 1894–1907, Mar. 2017.
- [2] NERC, "1,200 MW fault induced solar photovoltaic resource interruption disturbance report – southern California 8/16/2016 event," Jun. 2017, [Online]. Available: www.nerc.com.
- [3] NERC, "900 MW fault induced solar photovoltaic resource interruption disturbance report – southern California event: October 9, 2017," Feb. 2018, [Online]. Available: www.nerc.com.
- [4] E. O. N. Netz, "Grid code-high and extra high voltage," E. ON Netz GmbH, Bayreuth, Apr. 2006.
- [5] *Technical requirements for the connection and operation of customer installations to the high voltage network*, VDE-ARN 4120: 2018.
- [6] Ö. Göksu, R. Teodorescu, C. L. Bak, F. Iov and P. C. Kjør, "Impact of wind power plant reactive current injection during asymmetrical grid faults," *IET Renew. Power Gener.*, vol. 7, no. 5, pp. 484–492, Sep. 2013.
- [7] D. Dong, B. Wen, D. Boroyevich, and P. Mattavelli, "Analysis of phase-locked loop low-frequency stability in three-phase grid-connected power converters considering impedance interactions," *IEEE Trans. Ind. Electron.*, vol. 62, no. 1, pp. 310–321, Jan. 2015.
- [8] Ö. Göksu, R. Teodorescu, C. L. Bak, F. Iov, and P. C. Kjør, "Instability of wind turbine converters during current injection to low voltage grid faults and PLL frequency based stability solution," *IEEE Trans. Power Syst.*, vol. 29, no. 4, pp. 1683–1691, Jul. 2014.
- [9] X. He, H. Geng, J. Xi, and J. M. Guerrero, "Resynchronization analysis and improvement of grid-connected VSCs during grid faults," *IEEE J. Emerg. Sel. Top. Power Electron.*, in press.
- [10] X. He, H. Geng, R. Li, and B. C. Pal, "Transient stability analysis and enhancement of renewable energy conversion system during LVRT," *IEEE Trans. Sustain. Energy*, vol. 11, no. 3, pp. 1612–1623, Jul. 2020.
- [11] Q. Hu, L. Fu, F. Ma, and F. Ji, "Large signal synchronizing instability of PLL-based VSC connected to weak AC grid," *IEEE Trans. Power Syst.*, vol. 34, no. 4, pp. 3220–3229, Jul. 2019.
- [12] C. Zhang, M. Molinas, Z. Li, and X. Cai, "Synchronizing stability analysis and region of attraction estimation of grid-feeding VSCs using sum-of-squares programming," *Front. Energy Res.*, vol. 8, Apr. 2020.
- [13] H. Wu and X. Wang, "Transient stability impact of the phase-locked loop on grid-connected voltage source converters," in *Proc. IPEC-Niigata*, 2018.
- [14] J. Chen, M. Liu, T. O'Donnell, F. Milano, "Impact of current transients on the synchronization stability assessment of grid-feeding converters," *IEEE Trans. Power Syst.*, vol. 35, no. 5, pp. 4131–4134, Sep. 2020.
- [15] B. Weise, "Impact of K-factor and active current reduction during fault-ride-through of generating units connected via voltage-sourced converters on power system stability," *IET Renew. Power Gener.*, vol. 9, no. 1, pp. 25–36, Jan. 2015.
- [16] S. Ma, H. Geng, L. Liu, G. Yang, and B. C. Pal, "Grid-synchronization stability improvement of large scale wind farm during severe grid fault," *IEEE Trans. Power Syst.*, vol. 33, no. 1, pp. 216–226, Jan. 2018.
- [17] X. He and H. Geng, "Synchronization stability analysis and enhancement of grid-tied multi-converter systems," *2020 IEEE IAS Annual Meeting*.
- [18] L. B. Larumbe, *et al.*, "On the importance of tracking the negative-sequence phase-angle in three-phase inverters with double synchronous reference frame current control," *2020 IEEE ISIE*, Jun. 2020.
- [19] T. Neumann, *et al.*, "Enhanced dynamic voltage control of type 4 wind turbines during unbalanced grid faults," *IEEE Trans. Energy Convers.*, vol. 30, no. 4, pp. 1650–1659, Dec. 2015.
- [20] B. Wang, S. Wang, J. Hu, "Dynamic modeling of asymmetrical-faulted grid by decomposing coupled sequences via complex vector," *IEEE J. Emerg. Sel. Top. Power Electron.*, in press.
- [21] X. Bai, T. Jiang, Z. Guo, Z. Yan and Y. Ni, "A unified approach for processing unbalanced conditions in transient stability calculations," *IEEE Trans. Power Syst.*, vol. 21, no. 1, pp. 85–90, Feb. 2006.
- [22] S. Mortazavian and Y. A.-R. I. Mohamed, "Analysis and Augmented Model-Based Control Design of Distributed Generation Converters With a Flexible Grid-Support Controller," *IEEE Trans. Power Electron.*, vol. 34, no. 7, pp. 6369–6387, Jul. 2019.
- [23] X. He, H. Geng, G. Yang, "A generalized design framework of notch filter based frequency-locked loop for three-phase grid voltage," *IEEE Trans. Ind. Electron.*, vol. 65, no. 9, pp. 7072–7084, 2018.
- [24] N. Tleis, "Theory of symmetrical components and connection of phase sequence networks during faults," in *Power Systems Modelling and Fault Analysis - Theory and Practice*, 1st ed. Elsevier, 2008, ch. 2, sec. 3, pp. 28–73.
- [25] M. G. Taul, S. Golestan, X. Wang, P. Davari, and F. Blaabjerg, "Modeling of converter synchronization stability under grid faults: the general case," *IEEE J. Emerg. Sel. Top. Power Electron.*, in press.
- [26] J. Pei, J. Yao, R. Liu, D. Zeng, P. Sun, H. Zhang, and Y. Liu, "Characteristic analysis and risk assessment for voltage-frequency coupled transient instability of large-scale grid-connected renewable energy plants during LVRT," *IEEE Trans. Ind. Electron.*, vol. 67, no. 7, pp. 5515–5530, Jul. 2020.